

## Dynamics of crossover from a chaotic to a power-law state in jerky flow

M. S. Bharathi<sup>1</sup> and G. Ananthakrishna<sup>1,2</sup>

<sup>1</sup>Materials Research Centre, Indian Institute of Science, Bangalore-560012, India

<sup>2</sup>Centre for Condensed Matter Theory, Indian Institute of Science, Bangalore-560012, India

We study the dynamics of an intriguing crossover from a chaotic to a power-law state as a function of strain rate within the context of a recently introduced model that reproduces the crossover. While the chaotic regime has a small set of positive Lyapunov exponents, interestingly, the scaling regime has a power-law distribution of null exponents which also exhibits a power law. The slow-manifold analysis of the model shows that while a large proportion of dislocations are pinned in the chaotic regime, most of them are pushed to the threshold of unpinning in the scaling regime, thus providing an insight into the mechanism of crossover.

The Portevin Le-Chatelier (PLC) effect [1], or the jerky flow, is a rare example where the complex spatiotemporal dynamics results from the collective behavior of participating defects, namely, dislocations [2]. When samples (usually thin strips) of dilute alloys are subjected to constant strain rate deformation in a window of applied strain rates ( $\dot{\epsilon}_a$ ) and temperatures, one finds repeated stress drops (or yield drops). Each stress drop is associated with the formation of a band of dislocations. At low strain rates, the bands are static nucleating randomly in space. At intermediate  $\dot{\epsilon}_a$ , bands nucleate one ahead of the other in a hopping manner. At high strain rates, bands propagate continuously. The bands found in different regimes of strain rates are considered to be different correlated states of dislocations within the bands [3].

A classical explanation of the jerky flow is through dynamic strain aging [2]. At small velocities of dislocations (or  $\dot{\epsilon}_a$ ), solute atoms have sufficient time to diffuse to dislocations, and pin them. The longer they are arrested, the larger is the stress required to unpin them. As the stress increases, dislocations get unpinned and move fast till they are again pinned due to diffusing solutes and other pinning centers. The process repeats itself. Further, the competition between the time scales associated with diffusion and dislocation mobility translates, at the macroscopic level, to a negative strain rate sensitivity of the flow stress. This intermittent sequence of loading and unloading, and the negative flow rate sensitivity are typical features of many stick-slip situations such as fault dynamics [4], frictional sliding [5] and peeling of an adhesive tape [6], and charge density waves [7,8]. (Indeed, the similarity of the PLC effect with charge density waves has been studied in detail in Ref. [8].) The power-law statistics of stress drops [3,9] at *high*  $\dot{\epsilon}_a$  is similar to those in earthquakes [4] and many other power-law systems [10,11], which however are seen at *low* drives.

This rich spatiotemporal dynamics has defied a proper understanding due to the lack of techniques to describe the collective behavior of dislocations [2]. Recent studies using nonlinear dynamical methods have shown that a rich body of dynamical correlations is hidden in the stress-strain curves of jerky flow [12]. More recently, an *intriguing crossover* from a chaotic to a power-law regime has been observed as a function of strain rate [9,3]. As the crossover is seen in a single crystal and polycrystals, it appears to be insensitive to the microstructure.

This crossover is unusual in a number of ways. First, it is a *rare example of a transition between two dynamically distinct states*. Chaos is characterized by the self-similarity of the attractor and the sensitivity to initial conditions arising from a few degrees of freedom. In contrast, power laws are scale-free and are infinite dimensional. Thus, most systems exhibit either of these regimes. To the best of our knowledge, this is one of the two experimental situations where both are seen in the same system, the other being in the hydrodynamic turbulence [13]. Second, the power law in the PLC effect (as also in turbulence) is observed at *high drive rates*. On the other hand, power laws observed in varied systems, usually seen in *slowly driven* dissipative systems, are conventionally explained by invoking the concept of self-organized criticality (SOC) [10,11,14]. Thus, one suspects that the dynamical features of the power law here to be closer to turbulence than the conventional SOC systems.

Recently, we have succeeded in explaining this crossover in the dynamics of the PLC effect by extending the dynamical model for the PLC effect due to Ananthakrishna and co-workers [15,16]. The extended model also explains the three types of dislocation bands observed with the increasing strain rate [17]. However, the dynamics of the crossover has not been elucidated. A natural tool for characterizing the crossover is to follow the Lyapunov spectrum as a function of strain rate. This will be supplemented by the slow-manifold approach [18,19] that allows us get a geometrical picture of the changes occurring in the configuration of dislocations during crossover.

We shall briefly describe the extended dynamical [16] model. The original dynamical model [15] captures the well separated time scales implied in dynamic strain aging by using the fast mobile  $\rho_m(x,t)$ , immobile  $\rho_{im}(x,t)$ , and Cottrell types of dislocations  $\rho_c(x,t)$ . Then, all qualitative features of the effect emerge due to a nonlinear interaction of these populations, assumed to represent collective degrees of freedom. In spite of the idealized nature of the model, it has been successful in explaining several generic features of the effect, notably—the occurrence of the effect in a window of strain rates (or temperatures) and the emergence of negative strain rate sensitivity of the flow stress [15,18]. The model also predicts *chaotic stress drops* [20] that have been subsequently verified by analyzing experimental signals [9,12],

and hence has the right framework to model the crossover. The equation of motion of the scaled dislocation densities [15,18]  $\rho_m(x,t)$ ,  $\rho_{im}(x,t)$ , and  $\rho_c(x,t)$  are given by

$$\dot{\rho}_m = -b_0\rho_m^2 - \rho_m\rho_{im} + \rho_{im} - a\rho_m + \phi_{eff}^m\rho_m + (\mathcal{D}/\rho_{im}) \times [\phi_{eff}^m(x)\rho_m]_{xx}, \quad (1)$$

$$\dot{\rho}_{im} = b_0(b_0\rho_m^2 - \rho_m\rho_{im} - \rho_{im} + a\rho_c), \quad (2)$$

$$\dot{\rho}_c = c(\rho_m - \rho_c). \quad (3)$$

The overdot and the subscript  $x$  refer to the time and space derivatives, respectively. The first term in Eq. (1),  $b_0\rho_m^2$ , refers to the immobilization of two mobile dislocations due to the formation of locks,  $\rho_m\rho_{im}$  to the annihilation of a mobile dislocation with an immobile one,  $\rho_{im}$  to the remobilization of the immobile dislocation due to stress or thermal activation, and  $a\rho_m$  represents the immobilization of mobile dislocation due to the aggregation of solute atoms. Once a mobile dislocation starts acquiring solute atoms, we regard it as the Cottrell type  $\rho_c$ . These eventually become immobile as more solute atoms aggregate. The aggregation of solute atoms can be regarded as the definition of  $\rho_c$ , i.e.,  $\rho_c = \int_{-\infty}^t dt' \rho_m(t') \exp[-c(t-t')]$ . (See Ref. [18].)  $\phi_{eff}^m\rho_m$  refers to the rate of production of dislocations due to cross glide. This depends on the velocity of mobile dislocations taken to be  $V_m(\phi) = \phi_{eff}^m$ , where  $\phi_{eff} = (\phi - h\sqrt{\rho_{im}})$  is the scaled effective stress,  $\phi$  the scaled stress,  $m$  the velocity exponent, and  $h$  a work hardening parameter. In the original model, cross slip has been used as a source of dislocation multiplication which, however, is intrinsically nonlocal. During cross-slip dislocations, leave the slip plane due to, for instance, the effect of repulsive internal stresses and then slip back onto the slip plane. This mechanism transports dislocation densities through space. This is known to lead to a ‘‘diffusive-type’’ coupling [2]. Let  $\Delta x$  be an elementary length. Then, the flux  $\Phi(x)$  flowing from  $x \pm \Delta x$  and out of  $x$  is given by  $\Phi(x) + (p/2)[\Phi(x + \Delta x) - 2\Phi(x) + \Phi(x - \Delta x)]$ , where  $\Phi(x) = \rho_m(x)\phi_{eff}^m(x)$ . Here,  $p$  is the probability of spreading into neighboring elements. Expanding  $\Phi(x \pm \Delta x)$  up to the leading terms, we get  $\rho_m\phi_{eff}^m + (p/2)[\partial^2(\rho_m\phi_{eff}^m)/\partial x^2](\Delta x)^2$ . Since cross slip spreads only into regions of minimum back stress arising from  $\rho_{im}$  ahead of it, we use  $\Delta x^2 = \langle \Delta x^2 \rangle = \bar{r}^2\rho_{im}^{-1}$ . Here,  $\langle \rangle$  refers to the ensemble average and  $\bar{r}$  is an elementary (dimensionless) length with  $\mathcal{D} = p\bar{r}^2/2$ . The scaled constants,  $a$ ,  $b_0$ , and  $c$  refer, respectively, to the concentration of solute atoms slowing down the mobile dislocations, the reactivation of immobile dislocations, and the diffusion rate of solute atoms. The orders of magnitudes of these constants are known from the basic mechanisms and their correspondence with experimental quantities [18]. Defining  $\dot{\epsilon}$ ,  $d$ , and  $l$  as the scaled strain rate, effective modulus of the machine and the sample, and length of the sample, respectively, the machine equation reads

$$\dot{\phi} = d \left[ \dot{\epsilon} - (1/l) \int_0^l \rho_m(x,t) \phi_{eff}^m(x,t) dx \right]. \quad (4)$$

Global coupling in Eq. (4) is similar to the studies on space-charge currents in semiconductors where the integrated electric field balances the applied voltage.

In the domain of the crossover parameter  $\dot{\epsilon}$ , our earlier analysis [18,19] shows that the effect is observed between a forward Hopf bifurcation at low strain rate and a reverse one at high  $\dot{\epsilon}$ . The reverse Hopf bifurcation implies decreasing amplitudes of stress drops as in experiments. All the interesting dynamics, including chaos, is seen in this regime, as shown in Refs. [18,19].

We discretize the specimen length into  $N$  equal parts, and solve for  $\rho_m(j,t)$ ,  $\rho_{im}(j,t)$ ,  $\rho_c(j,t)$ ,  $j=1, \dots, N$ , and  $\phi(t)$ . Due to the widely differing time scales, appropriate care is taken in the numerical solutions by using a variable step fourth-order Runge-Kutta scheme with an accuracy of  $10^{-6}$  for all the variables. The spatial derivative is approximated by its central difference. The initial values are taken as the steady state values for the variables (as the long term evolution does not depend on the initial values) with a Gaussian spread along the length of the sample. In experiments, the ends of the sample have large strains induced due to high stress concentrations at the grips. To mimic the strain, we set  $\rho_{im}(j,t)$ ,  $j=1$ , and  $N$  to values two orders higher than the rest of the sample. Further, as bands cannot propagate into the grips, we use  $\rho_m(j,t) = \rho_c(j,t) = 0$  at  $j=1$  and  $N$ . For the numerical work, we use  $a=0.8$ ,  $b_0=0.0005$ ,  $c=0.08$ ,  $d=0.00006$ ,  $m=3.0$ ,  $h=0$ , and  $\mathcal{D}=0.5$ . However, the results hold true for a wide range of parameters values in the instability domain including that of  $\mathcal{D}$ . For these values, the PLC effect is seen in the range  $10 < \dot{\epsilon} < 2000$ . Chaotic and power law regimes are seen at low and high strain rates, respectively [16].

We identify the chaotic regime by calculating the Lyapunov exponents,  $\lambda_i$  ( $i=1, \dots, M=3N+1$ ), using Eqs. (1)–(4). (The various systems sizes studied from  $N=100$ –3333 show a rapid convergence of the results even around 300.) The largest Lyapunov exponent  $\lambda_1$  is obtained by averaging over 15 000 time steps after stabilization.  $\lambda_1$  becomes positive at  $\dot{\epsilon}=35$ , reaching a maximum at  $\dot{\epsilon}=120$ , and practically vanishes around 250. (See Fig. 3(a) of Ref. [16]. Periodic states are seen prior to chaos.) In the chaotic region, the distribution of Lyapunov exponents is quite broad. A plot for  $\dot{\epsilon}=120$  is shown Fig. 1(a). Of these, only 6.2% of  $M(=1051)$  are positive. As  $\dot{\epsilon}$  increases to 280, concomitant with the decrease in the maximum Lyapunov exponent to a small value  $\approx 5.2 \times 10^{-4}$ , the number of null exponents (almost vanishing) *increases gradually* reaching a value  $\approx 0.38M$  in the range  $[-0.00052, 0.00052]$  (compared to only a few for  $\dot{\epsilon}=120$ ). For  $\dot{\epsilon} \geq 250$ , below a resolution  $\sim 10^{-4}$ , even as the first few exponents are distinguishable, most cross each other as a function of time, but the (time averaged) distribution remains unaffected. The finite density of null exponents has a peaked nature in the

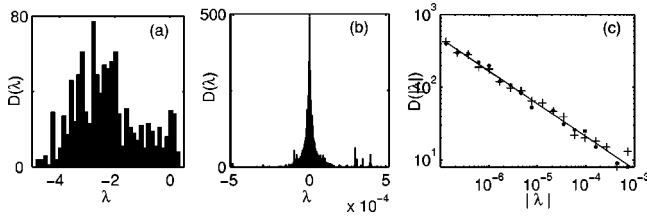


FIG. 1. (a) Distribution of the Lyapunov exponents at  $\dot{\epsilon}=120$  for  $M=1051$ . (b) and (c) Distribution of the null exponents at  $\dot{\epsilon}=280$  for  $M=10000$ . In (c) “+” refers to positive and “●” to negative null Lyapunov exponents.

interval  $250 \leq \dot{\epsilon} \leq 700$ . A plot is shown in Fig. 1(c) for  $\dot{\epsilon}=280$  which can be fitted to a power law  $D(|\lambda|) \sim |\lambda|^{-\gamma}$  as shown in Fig. 1(c) with  $\gamma=0.6$ . It may be pertinent to state here that the uncorrelated bands and hopping bands are seen in the chaotic regime, while the continuously propagating bands are seen at high strain rate [17].

As yield drops are caused by the unpinning of dislocations from the pinned configuration, we first need to identify these configurations. This can be done by using the slow-manifold approach. Here, we recall some relevant results [18,19] on the slow manifold of the original model ( $D=0$ ) for further use when  $D \neq 0$ . The slow manifold expresses the fast variable in terms of the slow variables, conventionally done by setting the derivative of the fast variable to zero [18,19]. Here,  $\dot{\rho}_m=0$  gives  $\rho_m = \rho_m(\rho_{im}, \phi)$ . Instead, we use  $\rho_m$  in terms of a single slow variable  $\delta = \phi^m - \rho_{im} - a$ . We note that  $\delta$  takes on small positive and negative values, since both  $\rho_{im}$  and  $\phi$  are small and positive. Using  $\dot{\rho}_m = g(\rho_m, \phi) = -b_0 \rho_m^2 + \rho_m \delta + \rho_{im} = 0$ , and noting that  $\rho_m > 0$ , we get two solutions  $\rho_m = [\delta + (\delta^2 + 4b_0 \rho_{im})^{1/2}] / 2b_0$ , one for  $\delta < 0$  and another  $\delta > 0$ . For regions of  $\delta < 0$ , since  $b_0$  is small  $\sim 10^{-4}$ , we get  $\rho_m / \rho_{im} \approx -1/\delta$  which takes on small values defining a part of the slow manifold,  $S_2$ . Since physically pinned configuration of dislocations implies small mobile density and large immobile density, we refer to the region of  $S_2$  as the “pinned state of dislocations.” Further, larger negative values of  $\delta$  correspond to strongly pinned configurations, as they refer to a smaller ratio of  $\rho_m / \rho_{im}$ . Corresponding to  $\delta > 0$ , another connected piece  $S_1$  is defined by large values of  $\rho_m$ , given by  $\rho_m \approx \delta / b_0$ , which we refer to as the “unpinned state of dislocations.”  $S_2$  and  $S_1$  are separated by  $\delta=0$ , which we refer to as the *fold line* [18,19] (see below). A plot of the slow manifold in the  $\delta$ - $\rho_m$  plane is shown in Fig. 2(a) along with a simple monoperoiodic trajectory describing the changes in the densities during one loading-unloading cycle. The inset shows  $\rho_m(t)$  and  $\phi(t)$ . For completeness, the corresponding plot of the slow manifold in the  $(\rho_m, \rho_{im}, \phi)$  space is shown in Fig. 2(b), along with the trajectory and the symbols. Note that  $S_2$  and  $S_1$  are separated by  $\delta = \phi^m - \rho_{im} - a = 0$ , and hence the name fold line. In Fig. 2(a), as the trajectory enters  $S_2$  at  $A$  and moves into  $S_2$ ,  $\delta$  takes a maximum negative value at  $B$ . Then,  $\delta$  increases as the trajectory returns to  $A'$  before leaving  $S_2$ . The corresponding segment is  $ABA'$  in Fig. 2(b), which is identified with the flat region of  $\rho_m(t)$  in the inset of Fig.

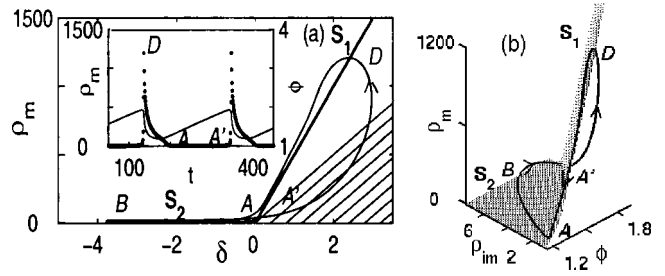


FIG. 2. (a) Bent slow manifold  $S_1$  and  $S_2$  (thick lines) with a simple trajectory for  $\dot{\epsilon}=200$  and  $m=3$ . Inset:  $\rho_m$  (dotted curve) and  $\phi$ . (b) Same trajectory in the  $(\phi, \rho_{im}, \rho_m)$  space.

2(a). As the trajectory crosses  $\delta=0$ ,  $\partial g / \partial \rho_m$  becomes positive and it accelerates into the shaded region [Fig. 2(a)] rapidly till it reaches  $\rho_m = \delta / 2b_0$ . Thereafter, it settles down quickly on  $S_1$  decreasing rapidly till it reenters  $S_2$  again at  $A$ . The burst in  $\rho_m$  [inset in Fig. 2(a)] corresponds to the segment  $A'DA$  in Figs. 2(a) and 2(b).

Now consider the stress changes as the state of the system goes through a burst of plastic activity. For  $D=0$ , Eq. (4) reduces to  $\dot{\phi} = d[\dot{\epsilon} - \dot{\epsilon}_p]$ , where  $\dot{\epsilon}_p = \phi^m \rho_m$  defines the plastic strain rate. Since  $\rho_m$  is small and nearly constant at  $S_2$ , stress increases monotonically. However, during the burst in  $\rho_m$  ( $A'DA$  in the inset),  $\dot{\epsilon}_p(t)$  exceeds  $\dot{\epsilon}$  leading to an yield drop. Since  $\rho_m$  grows outside  $S_2$ ,  $\delta=0$  separates the pinned state from the unpinned state, and hence  $\delta=0$  physically corresponds to the value of the effective stress at which dislocations are unpinned.

Now, we extend the slow-manifold analysis to the case when spatial coupling  $D \neq 0$  to study the changes in the spatial configuration of dislocations as we go from the chaotic to scaling regime. Using  $h=0, \phi_{eff} = \phi$ , the plastic strain rate  $\dot{\epsilon}_p(t) = \phi^m(t) (1/l) \int_0^l \rho_m(x,t) dx = \phi^m(t) \bar{\rho}_m(t)$ , where  $\bar{\rho}_m(t)$  is the mean mobile density  $[\bar{\rho}_m(t) = \sum_j \rho_m(j,t) / N]$ . Thus, the yield drop is controlled by the spatial average  $\bar{\rho}_m(t)$  and not by individual values of  $\rho_m(j)$ . Since the yield drop occurs when  $\bar{\rho}_m(t)$  grows rapidly, it is adequate to examine the spatial configurations on the slow manifold at the onset and at the end of typical yield drops. Figures 3(a), and 3(b) and 3(c) and 3(d) show, respectively, the plots of  $j, \delta(j), \rho_m(j)$  for the chaotic state  $\dot{\epsilon}=120$  and the power-law state  $\dot{\epsilon}=280$ , at the onset and at the end of an yield drop. It is clear that for  $\dot{\epsilon}=120$ , both at the onset and at the end of a typical large yield drop [Figs. 3(a) and 3(b)], most  $\rho_m(j)$ 's are small with large negative values of  $\delta(j)$ , i.e., most dislocations are in a strongly pinned state. The arrows show the increase in  $\rho_m(j)$  at the end of the yield drop. In contrast, in the scaling regime, for  $\dot{\epsilon}=280$ , most dislocations are at the threshold of unpinning with  $\delta(j) \approx 0$ , both at the onset and the end of the yield drop [Figs. 3(c) and 3(d)]. This also implies that they remain close to this threshold *all the time* [Fig. 3(d)]. Since  $\delta(j) \approx 0$  (for most  $j$ 's) refers to a marginally stable state, it can produce almost any response. This in turn implies that the magnitudes of yield drops  $\Delta \phi$  are scale-free. We have verified that the edge-of-unpinning picture is valid in the entire scaling regime for a range of  $N=100-1000$ . Further,

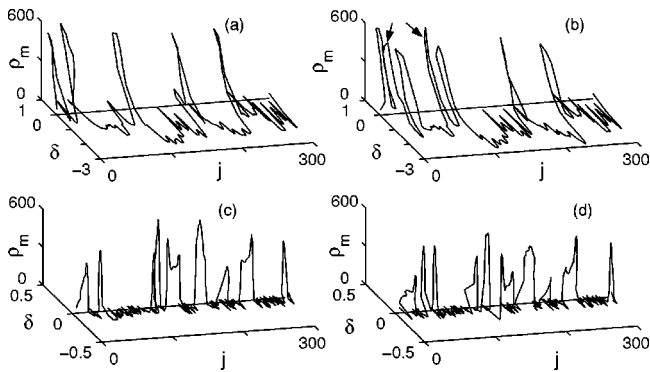


FIG. 3. Dislocation configurations on the slow manifold at the inset and at the end of an yield drop: (a) and (b) for  $\dot{\epsilon} = 120$  (chaos), and (c) and (d) for  $\dot{\epsilon} = 280$  (scaling).

the number of spatial elements reaching the threshold of unpinning  $\delta = 0$  during an yield drop increases as we approach the scaling regime.

Several comments may be in order on the dynamics of the crossover. First, the crossover itself is smooth as the changes in the Lyapunov spectrum are gradual. Second, the power law here is of purely dynamical origin. This is a result of the reverse Hopf bifurcation at high strain rates which limits the average stress drop amplitude to small values [18,19]. Third, our analysis shows that the power-law regime of stress drops occurring at high strain rates belongs to a different universality class as it is characterized by a dense set of null exponents. As zero exponents correspond to a marginal situation, their finite density physically implies that most spatial elements are close to criticality. This is supported by the geometrical picture of the slow manifold, where most disloca-

tions are at the threshold of unpinning,  $\delta = 0$ . In contrast, going by the few reports, the marginal nature of conventional SOC models does not display any characteristic feature in the Lyapunov spectrum [21]. (For instance, no zero and positive exponents, a positive and zero exponent, zero exponent in the large- $N$  limit, etc., have been reported [21].) More significantly, the dense set of null Lyapunov exponents themselves follow a power law. Further, we note that the Lyapunov spectrum evolves from a set of both positive and negative, but few null exponents in the chaotic region, to a dense set of marginal exponents as we reach the power-law regime. Thus, the dense set of null exponents in our model is actually similar to that obtained in shell models of turbulence where the power law is seen at high drive values [22]. However, there are significant differences. First, we note that the shell model [22] cannot explain the crossover as it is only designed to explain the power-law regime. Further, the maximum Lyapunov exponent is large for small viscosity parameter,  $\nu$ , ( $\lambda_1 \propto \nu^{1/2}$ ) in shell models [22] in contrast to near-zero value in our model.

In conclusion, we have demonstrated that the changes in the Lyapunov spectrum provides a good insight into the dynamical mechanism controlling the crossover. The slow-manifold analysis, applied to study the crossover, is particularly useful in giving a geometrical picture of the spatial configurations in the chaotic and scaling regimes. This picture explains the origin of small amplitude stress drops at high strain rates. Finally, this presents a fully dynamical model which exhibits a crossover from a chaotic to a power-law regime and should be of interest to the area of dynamical systems.

This work was supported by the Department of Science and Technology, New Delhi, India.

- 
- [1] F. Le Chatelier, *Rev. Métall.* **6**, 914 (1909).  
 [2] L.P. Kubin *et al.*, in *Collective Behavior of Dislocations*, edited by F.R.N. Nabarro and M.S. Deussery, *Dislocations in Solids Vol. 11* (North-Holland, Amsterdam, 2002).  
 [3] M.S. Bharathi *et al.*, *Phys. Rev. Lett.* **87**, 165508 (2001).  
 [4] R. Burridge and L. Knopoff, *Bull. Seismol. Soc. Am.* **57**, 3411 (1967).  
 [5] B.N.J. Persson and E. Tosatti, *Physics of Sliding Friction* (Kluwer Academic, Dordrecht, 1996).  
 [6] D. Maugis and M. Barquins, in *Adhesion*, edited by K.W. Allen (Elsevier, London, 1988), Vol. 12.  
 [7] C. Tang *et al.*, *Phys. Rev. Lett.* **58**, 1161 (1987).  
 [8] J. Dumas and D. Feinberg, *Europhys. Lett.* **2**, 555 (1986).  
 [9] G. Ananthakrishna *et al.*, *Phys. Rev. E* **60**, 5455 (1999).  
 [10] P. Bak, C. Tang, and K. Wiesenfeld, *Phys. Rev. Lett.* **59**, 381 (1987); *Phys. Rev. A* **38**, 364 (1988).  
 [11] H.J. Jensen, *Self-Organized Criticality* (Cambridge University Press, Cambridge, 1998).  
 [12] S.J. Noronha *et al.*, *Int. J. Bifurcation Chaos Appl. Sci. Eng.* **7**, 2577 (1997), and the references therein.  
 [13] See, for instance, F. Heslot, B. Castaing, and A. Libchaber, *Phys. Rev. A* **36**, 5870 (1987).  
 [14] P. Bak, *How Nature Works* (Springer-Verlag, New York, 1996).  
 [15] G. Ananthakrishna and M. C. Valsakumar, *J. Phys. D* **15**, L171 (1982).  
 [16] M.S. Bharathi and G. Ananthakrishna, *Europhys. Lett.* **60**, 234 (2002).  
 [17] M.S. Bharathi, S. Rajesh, and G. Ananthakrishna, *Scr. Mater.* **48**, 1355 (2003).  
 [18] S. Rajesh and G. Ananthakrishna, *Phys. Rev. E* **61**, 3664 (2000).  
 [19] S. Rajesh and G. Ananthakrishna, *Physica D* **140**, 193 (2000).  
 [20] G. Ananthakrishna and M.C. Valsakumar, *Phys. Lett.* **95A**, 69 (1983).  
 [21] A. Erzan *et al.*, *Phys. Rev. Lett.* **66**, 2750 (1991); M. de Sousa Vieira *et al.*, *Phys. Rev. E* **53**, 1441 (1996); B. Cessac, *et al.*, *ibid.* **64**, 016133 (2001).  
 [22] M. Yamada and K. Ohkitani, *J. Phys. Soc. Jpn.* **56**, 4210 (1987); A. Cristani *et al.*, *Physica D* **76**, 239 (1994).